CHALMERS
UNIVERSITY OF TECHNOLOGY

Steam methane reforming with chemical-looping combustion: Scaling of fluidized-bed-heated reformer tubes

energy&fuels

pubs.acs.org/EF

Article

Steam Methane Reforming with Chemical-Looping Combustion: Scaling of Fluidized-Bed-Heated Reformer Tubes

Tobias Pröll* and Anders Lyngfelt

Cite This: *Energy Fuels* 2022, 36, 9502−9512

Read Online

ACCESS | Metrics & More | Article Recommendations

ABSTRACT: The combination of chemical-looping combustion (CLC) and steam methane reforming (SMR) bears the potential for quantitative and energy-efficient CO_2 capture along with hydrogen production from natural gas. A 2-dimensional axisymmetric model of a SMR tube was used to estimate the possibility to adapt the tube dimensions to better fit into fluidized-bed heat exchangers. A constant surrounding fluidized-bed temperature was set as the boundary condition. There are two phenomena that affect the reactor performance: the effective heat-transfer rate from the fluidized bed to and through the tube wall and onward to and into the catalyst bed on the one hand and the effective reaction rates of the governing chemical reactions on the other hand. Literature models were used for the heat-transfer description assuming a state-of-the-art reforming catalyst and classical SMR kinetics were formulated. The simulation results show a temperature decrease toward the tube center in steady state operation. The gas phase composition at the tube outlet reflects the radial temperature distribution as the chemical equilibrium is approached well. Simulations with smaller tube diameters indicate that the necessary tube length for equivalent gas conversion is significantly reduced. In a 1/2-scale setting with 63 mm inner diameter (ID) of the tube instead of 126 mm ID in full scale, the necessary tube length is only 6.0 m instead of 12.5 m, and in a 1/4-scale setting with 31.5 mm ID, the necessary tube length is only 3.3 m. A temperature increase of the fluidized bed from 900 to 950 and 1000 °C may reduce the necessary tube length in the 1/4 scale from 3.3 to 2.6 and 2.2 m, respectively. These indications are promising with respect to the possibilities for fluidized-bed immersed reformer tube dimensioning and arrangement. More detailed reactor design studies will be necessary to judge the industrial feasibility of the CLC-SMR combination.

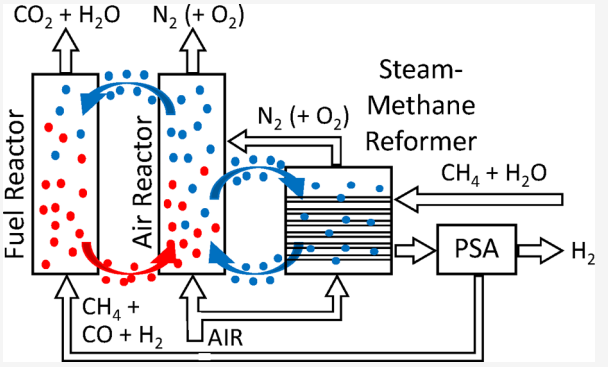

1. INTRODUCTION

1.1. Steam Methane Reforming (SMR) for Synthesis Gas and Hydrogen Production. The most common way to produce hydrogen is steam methane reforming (SMR) of natural gas.[1] The process involves the reaction between steam and methane to produce a syngas, a subsequent process step called water−gas shift (WGS), where the hydrogen content is increased by the reaction of H_2O with CO at lower temperatures and, finally, hydrogen is extracted from the gas using pressure swing adsorption (PSA). Remaining off-gas is burnt with additional natural gas to provide the heat needed for the SMR. In the classical SMR process with PSA according to Figure 1, the CO_2 is contained in the reactive furnace exhaust gas in diluted form. Capture and concentration of CO_2 could be done using a postcombustion CO_2 capture system. Postcombustion capture of CO_2 from the dilute stream such as amine scrubbing or temperature swing adsorption would come with a relevant additional energy demand. Alternative process configurations in chemical industry apply low-temperature physical scrubbing processes instead of PSA for the separation of hydrogen and CO_2 (Rectisol or Selexol processes). In these cases, the CO_2 from the synthesis gas is readily available in concentrated form and can be used, for example, for urea synthesis whereas the CO_2 from the reactive furnace is still contained in the flue gas. The two elementary reactions taking place inside the reformer tubes are the steam reforming reaction 1 and the water−gas-shift reaction 2. Combination of (1) and (2) leads to the overall reaction 3 that may also happen as one elementary step.

$$CH_4 + H_2O \leftrightarrow CO + 3H_2 \quad (1)$$

$$CO + H_2O \leftrightarrow CO_2 + H_2 \quad (2)$$

$$CH_4 + 2H_2O \leftrightarrow CO_2 + 4H_2 \quad (3)$$

Special Issue: 2022 Pioneers in Energy Research: Anders Lyngfelt

Received: April 9, 2022
Revised: June 30, 2022
Published: July 21, 2022

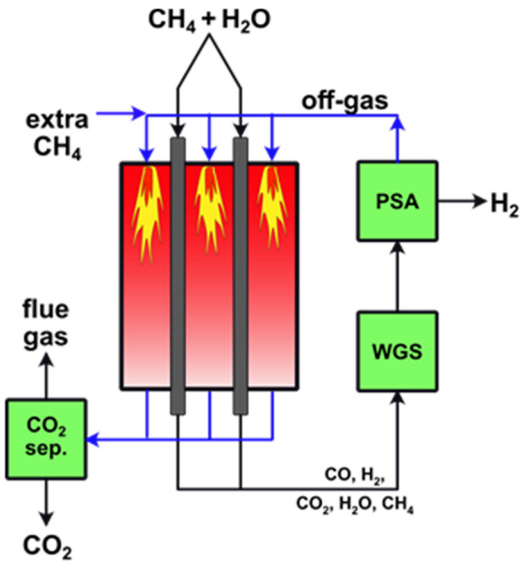

Figure 1. Schematic of classical steam methane reforming (SMR) with a postcombustion CO_2 capture system.

SMR is carried out in tubular reactors filled with catalyst where the inside gas temperature may vary from 600 to 900 °C, with the heat provided by radiation from high-temperature flames outside the tubes (Figure 1).

To achieve sufficient heat transfer, the temperature of the gases leaving the furnace is high, typically around 1200 °C. Thus, a major part of the heat produced by the combustion leaves the furnace instead of being utilized for the SMR. High temperatures of flames in combination with a varying gas temperature and heat consumption inside the tubes means that the tubes are exposed to harsh conditions, and local hot spots may cause damage to the expensive tubes and catalyst. As an optimum for the technology, an operating pressure of 30 bar and tube dimensions of 10−13 m length and 10−13 cm inner diameter have been established during the last decades. It is important to notice that the SMR process operates under relevant constraints:

- Increased pressure (30 bar) is desired because the synthesis gas is required at high pressure for downstream processes.
- High temperatures (750−850 °C) and catalysts are required to facilitate the endothermic reforming reaction thermodynamically and kinetically.
- Heat needs to be supplied through the reformer tube shell and through heat transfer in the catalyst bed.
- Sulfur tolerance of the catalyst is improved, but energy efficiency is decreased with increasing operating temperatures.

To decarbonize the SMR process, CO_2 capture and storage (CCS) concepts can be applied. Although it is less difficult to capture and concentrate CO_2 from the high-pressure-synthesis gas stream, the flue gas from the reactive furnace also needs to be stripped of CO_2 to obtain CO_2-free hydrogen. The state-of-the-art for CO_2 capture is to wash the gas with monoethanol amine (MEA) or a similar absorbent dissolved in water. The absorbent is regenerated by heating the liquid, whereby the CO_2 is released. With MEA, the regeneration step requires around 3.9 MJ/kg of CO_2, to be compared to the heating value of methane, which is 18.2 MJ/kg of CO_2.[2] As said, CO_2 can also be removed from the process stream, for example, before or after the PSA. Although pressure and concentration are higher, there is nevertheless the need to regenerate the absorbent, even if the specific energy demand for CO_2 capture is somewhat lower at these conditions.

1.2. Chemical-Looping Combustion (CLC) Integrated with SMR. To avoid the energy penalty associated with the CO_2 capture, Rydén and Lyngfelt[3] proposed an integrated process configuration with chemical-looping combustion (CLC) of gaseous fuels and reformer tubes arranged inside a fluidized bed. The process configuration in Figure 2 deviates from the original

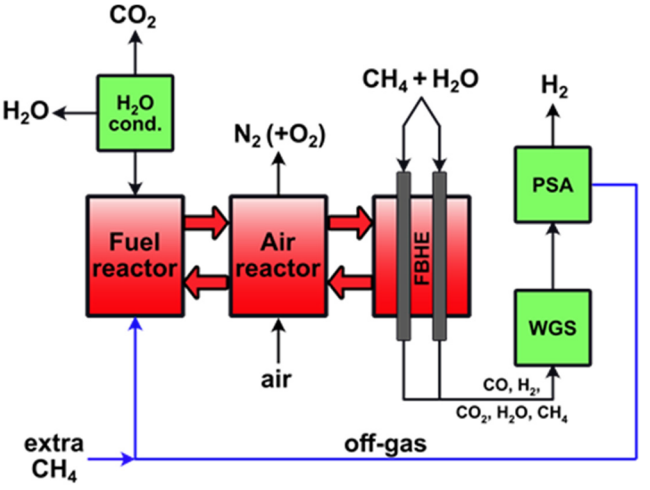

Figure 2. Chemical-looping combustion integrated with steam methane reforming (CLC-SMR). This figure was reproduced with permission from ref 5. Copyright 2022 The Authors.

proposal as the reformer tubes are arranged in a separate vessel, the fluidized-bed heat exchanger (FBHE) that is connected to the lower part of the air reactor via a circulating particle stream. Though the air reactor and the fuel reactor are typically circulating fluidized-bed (CFB) reactors, the FBHE can be designed as a dense bubbling fluidized bed to allow for effective heat transfer while keeping erosion effects low. Such systems, where bubbling-bed heat exchangers for steam generation or steam superheating are connected to CFB risers, are widely used in industry today. Thus, all CFB boilers for waste incineration from Andritz use adiabatic risers and all the cooling is in the external FBHE.[4] The necessary solids circulation between air reactor and FBHE as well as between air reactor and fuel reactor could be achieved through collection of the downward flowing solids in the lower part of the air reactor riser.[5] The major undertaking needed for an integration of SMR in CLC is optimization of the arrangement of reformer tubes of sufficient size in a FBHE.

Chemical-looping combustion (CLC) is a process where the oxygen is transferred from the air to the fuel using an oxygen carrier, circulating between the air reactor and the fuel reactor. Ideally, the exhaust from the fuel reactor only contains CO_2 and H_2O, the latter easily removed by condensation. Thus, pure CO_2 can be obtained without any costly and energy demanding gas separation. The exhaust from the air reactor is just air that has lost most of its oxygen content.

If the high-temperature furnace used for burning off-gas and methane for heating the steam reforming tubes is replaced by chemical-looping combustion, CO_2 can be captured without a costly and energy demanding gas separation process. An additional advantage with SMR-CLC is that the heat can be transferred to the steam reforming tubes using fluidized-bed

https://doi.org/10.1021/acs.energyfuels.2c01086
Energy Fuels 2022, 36, 9502−9512

heat exchangers (FBHE) with high heat transfer and low excess temperature. Thus, the temperature of the outgoing flue gases can be reduced from, for example, 1200 to 935 °C and the overall energy efficiency of the process is likely raised at the same time as CO_2 is quantitatively captured.[6] This is explained by two combined advantages, first, that the CLC process inherently captures CO_2 without the high energy penalty pertaining to gas separation and, second, that the much lower outlet temperature of the combustion chamber means that much more of the heat generated can be used for the reforming. A techno-economic analysis also indicates that the cost of producing hydrogen can be lowered compared to the cost of conventional SMR, which, if so, means that the CO_2 capture cost is negative.[6]

A further advantage is that CLC-SMR can eliminate NO_x emissions because no thermal NO_x is formed in the air reactor and the absence of any nitrogen compounds other than N_2 in the natural gas will prevent the formation of fuel-NO_x in the fuel reactor.

1.3. Technology Readiness of Chemical-Looping Combustion. There is no commercial-size experience of chemical-looping combustion. However, more than 12000 h of operation in smaller pilots has been reported.[7,8] The operation involves gaseous, solid, and liquid fuels as well as a large number of different oxygen-carrier materials. The work involves both manufactured materials and low-cost natural ores or waste materials. Low-cost materials often have high reactivity with syngas, but poor reactivity with methane.

A CLC reactor system involves two interconnected fluidized beds and would have large similarities to circulating fluidized-bed (CFB) boilers. Lyngfelt et al.[5] proposed that the scale-up to commercial size would involve a combined CFB-CLC boiler of 200 MW_{th}, basically a CFB with an added fuel reactor. They also concluded that the added costs for building and operating such a system would be smaller than building and operating an intermediate size of CLC unit of 10−30 MW_{th}. Additional advantages would be reaching full scale much quicker and having a fall-back option to operate the unit as a CFB for the worst-case scenario where CLC would not meet expectations. Such a combined system could be used to optimize operation and would also be able to switch gradually from CFB to CLC operation.

The addition of a fuel reactor should not be very expensive, as it consists of empty space and uncooled walls. For a 200 MW_{th} CLC, around 1300 m^2 of wall is needed for fuel reactor, downstream cyclone, and postoxidation chamber. At a cost of 1500 €/m^2 wall, the investment would be around 2 M€.[5,9] If used for CO_2 capture, this investment would give a cost of around 0.5 €/t CO_2, which is 2 orders of magnitude less than the costs of other capture technologies. The main costs for CLC are CO_2 compression and, in the case of incomplete gas conversion, oxygen polishing of the gas from the fuel reactor.[5,9]

The key challenges for a CLC system include adequate circulation, an oxygen carrier that can perform its duty to transfer oxygen without being mechanically or chemically deteriorated, and finally a downstream system where the CO_2 coming from the fuel reactor is upgraded to transport and storage quality.

A study of commercial CFB boilers indicated that the actual circulation was 5−50% of that needed in CLC.[5] It is not really a goal for CFBs to have high circulation, as this also increases the duty of the cyclones to properly capture and return the particles. It is also evident that circulation can be dramatically increased by lowering the particle size of the bed materials. Nevertheless, the study proposed a system where the downfall along the walls of the air reactor would be collected as being more reliable.

Experiences from more than 3400 h of operation in pilots using low-cost materials verify that many materials, such as ilmenite and manganese ores, have estimated lifetimes of several hundred hours,[5] which would translate to a low oxygen carrier cost (i.e., a few € per ton of CO_2 captured).[9] These materials would, however, have difficulties in reaching high conversion of methane.

However, there are manufactured materials that can reach full gas conversion, such as calcium manganate ($CaMnO_3$) and materials with supported copper oxide. These materials spontaneously release oxygen in the fuel reactor, where it is rapidly consumed. The concept of using oxide systems with an equilibrium oxygen pressure around 1−3%, which make them able to absorb oxygen in the air reactor and release oxygen in the fuel reactor is called chemical looping with oxygen uncoupling (CLOU).[10,11] More than 700 h of pilot operation with calcium manganate has shown that it is possible to reach full conversion and a slight surplus of oxygen.[12−25] Moreover, such materials have shown low attrition, with estimated lifetimes in the order of 10000 h. It should also be possible to produce calcium manganate from low-cost raw materials, such as limestone and manganese ore. Production of such materials up to a few tonnes have been demonstrated,[26] although more efforts would be needed get to multitonne production.

Another possibility is to add steam to the gas going to the fuel reactor, heat the gas, and pass it through a reformer tube to convert the methane to CO and H_2. Syngas has high reactivity with low-cost natural minerals. Sundqvist examined 19 manganese ores and eight of these showed a CO conversion of around 90% with exposure to syngas.[27] Hydrogen conversion was not measured, but previous experiences indicate that hydrogen is always more reactive and can be expected to have higher or even full conversion. The work was done with 2 g of oxygen carrier diluted in inert sand and at a fuel flow of 0.45 L_n/min, which corresponds to 23 kg/MW. This would amount to around 230 kg/m^2 or a pressure drop of only 2.2 kPa in a full-scale CFB-type fuel reactor. Assuming the fuel reactor operates at a pressure drop of 10 kPa with high circulation (i.e., a significant pressure drop along the height of the riser giving good gas−solids contact), very high conversion would be expected. A further advantage with pre-reforming of the fuel gas is that the endothermic reaction in the reformer would yield a fuel giving exothermic reactions in the fuel reactor. It is well-known that the reactions of both CO and H_2 with ilmenite, iron, and manganese ores are exothermic. Thus, the fuel reactor could be operated at a higher temperature (i.e., more similarly to the air reactor), which would also be helpful for the gas conversion.

The downstream treatment involves oxy-polishing, to remove any combustibles, cooling, particle removal, steam condensation, and removal of impurities like O_2 and NO that need to be removed from the CO_2 before transportation and storage. One option is to remove water-soluble gases in the condensation steps and thus remove gases like O_2 and NO by distillation in connection with the compression of the CO_2 stream. Distillation of gas from oxy combustion was investigated by Dickmeis and Kather,[28] indicating that it should be possible to reach low O_2 and NO.

For a CLC-SMR process, the temperatures needed are higher than normal CFB combustion. However, CLC pilot operation at higher temperatures is normal, and for example, a solid-fuel-fired

https://doi.org/10.1021/acs.energyfuels.2c01086
Energy Fuels 2022, 36, 9502−9512

Table 1. Geometric Data and Model Parameters for the Different Cases Investigated in This Study

parameter	unit	full scale	1/2 scale	1/4 scale		
reformer tube length	m	12.5	<12.5	<12.5		
reformer tube inner diameter	m	0.126	0.063	0.0315		
reformer tube inner cross-section	m^2	12.5×10^{-3}	3.12×10^{-3}	0.78×10^{-3}		
tube/catalyst diameter ratio		19.7	9.8	4.9		
porosity of solids packing		0.416	0.432	0.464		
steam-carbon molar ratio inlet	mol/mol	3.0	3.0	3.0		
mass flow gas	kg/s	0.116	0.029	0.0072		
pressure gas	bar	30	30	30		
reformer tube gas inlet temperature	°C	600	600	600		
outside fluidized-bed temperature	°C	900	900	900	950	1000
fluidized-bed−wall heat-transfer coeff	$W/(m^2 \cdot K)$	795	795	795	820	851
inner-wall−catalyst-bed heat transfer coeff	$W/(m^2 \cdot K)$	769	808	892	892	892
effective radial heat conductivity	W/(m·K)	21.0	18.5	15.5	15.5	15.5
effective axial heat conductivity	W/(m·K)	84.8	84.8	84.8	84.8	84.8

100 kW pilot normally operates at a temperature of 1025 °C.[29−34]

1.4. Problem Definition for the Present Work. According to Rydén and Lyngfelt,[3] the "marriage between SMR and CLC" promises high CO_2 capture efficiency at low energy penalties. To build such a system, reformer tubes need to be placed inside a fluidized-bed reactor for effective heat transfer from the fluidized bed toward the reformer tubes. It is evident that tubes longer than 10 m cannot easily be arranged inside a fluidized bed. From the perspective of SMR, vertical tubes are preferred for easy catalyst handling. Therefore, within the present contribution, we pose the following research questions:

- How can the dimensions of the reformer tubes be changed to fit better into a CLC fluidized-bed system?
- How does the tube diameter affect the necessary tube length?

The background of the second research question is the hypothesis that heat transfer is a significant limitation in the classical SMR process determining the tube-length requirement. This means that the heat transfer from the wall toward the center of the reformer tube limits the conversion of the endothermic overall reforming reaction. In such a case, smaller tube diameters would consequently allow for shorter tubes to achieve a comparable conversion performance. A recent article by Wang et al.[36] indicates that the local gas concentration inside a full-scale reformer tube correlates well with the temperature profile. Thus, a 2D axisymmetrical parametric model of a reformer tube was used in the present work to investigate the effect of geometrical changes (i.e., the tube diameter) on temperature distribution and gas conversion performance.

2. METHODOLOGY

2.1. Model Structure and Assumptions. The heat balance was formulated for the catalyst bed on the basis of heat conduction in the fixed bed described by an average effective heat conductivity k_{eff} considering gas throughflow and the chemical reactions 1, 2, and 3. A pseudohomogeneous model[35] with local temperature identity between gas and catalyst is assumed, which seems appropriate with respect to the small temperature differences between gas and catalyst reported, for example, by Wang et al.[36] The temperature of the surrounding fluidized bed was set to a defined value as the boundary condition. The heat transfer from the fluidized bed to the outer-tube wall was calculated according to Martin[37] and the heat transfer from the inner tube wall to and into the catalyst packing was calculated according to the h_w approach recommended by Tsotsas.[38] The intrinsic reaction rates were formulated strictly according to Xu and Froment[39] and an overall constant effectiveness factor for all reactions was assumed to 0.02, inspired by the results of Xu and Froment.[40] The detailed model equations are summarized in section 2.3. The local chemical equilibrium is calculated for each of the modeled reactions as an indicator whether heat transfer or the chemical reaction limits the overall process. The 2D axisymmetric model was implemented as a structured script in MATLAB. The CH_4 conversion and H_2 yield along the length axis were defined from average molar flows of gas species in the relevant cross-section:

$$X_{CH_4} = 1 - \frac{2\pi \int_{r=0}^{R} j_{CH_4}(r) \cdot r \, dr}{\dot{n}_{CH_4,in}} \tag{4}$$

$$Y_{H_2} = \frac{2\pi \int_{r=0}^{R} j_{H_2}(r) \cdot r \, dr}{4 \cdot \dot{n}_{CH_4,in}} \tag{5}$$

The local deviation from equilibrium V_{eq} is calculated from the partial pressures of the species involved and the partial pressure equilibrium constant of reactions 1 and 2:

$$V_{Eq,1} = \frac{\frac{p_{CO} \cdot p_{H_2}^{\ 3}}{p_{CH_4} \cdot p_{H_2O}}}{K_{p,1}(T)} \tag{6}$$

$$V_{Eq,2} = \frac{\frac{p_{CO2} \cdot p_{H_2}}{p_{CO} \cdot p_{H_2O}}}{K_{p,2}(T)} \tag{7}$$

In the results section, the decadal logarithm of V_{Eq} will be displayed. Values of $^{10}\log(V_{Eq})$ below the zero mean that the local species distribution is on the side of the reactants and reaction progress toward the products is possible. A value of zero means that the respective reaction is in equilibrium.

2.2. Model Parameters and Procedure. For the fluidized-bed heat-transfer parameters, ilmenite particles with a Sauter mean diameter of 180 μm and a hydrodynamic particle density of 3700 kg/m^3 were assumed in moderate fluidization with a fluidization number $u_0/u_{0,mf}$ of 5. Fluid properties of air at 1 bar pressure and operating temperature were assumed for the

https://doi.org/10.1021/acs.energyfuels.2c01086
Energy Fuels 2022, 36, 9502−9512

fluidized-bed heat-transfer calculation according to Martin.[37] The tube shell was modeled according to Dixon[41] with a heat conductivity in the steel shell of 1 W/(m·K). Geometric data of a state-of-the-art reforming catalyst Haldor Topsoe R67-7H were used according to Pedernera et al.[42] leading to an equivalent particle diameter of 6.4 mm.[36] The effects of changing tube diameter to catalyst particle diameter ratios on the average voidage of the catalyst bed and the inner wall to catalyst bed heat-transfer coefficient and effective radial heat conductivity in the bed were calculated strictly according to the procedure recommended by Tsotsas.[38]

The process was studied for a full-scale reformer tube with an inner diameter of 126 mm and a length of 12.5 m, for 50% inner tube diameter (1/2 scale) and for 25% inner tube diameter (1/4 scale). Table 1 summarizes bulk geometric data and preassessed model parameters for the investigated reformer tube settings. The "full-scale" reformer tube is aligned with the geometry, mass flow and molar steam/carbon ratio described by Wang et al.[36] The "1/2-scale" reformer tube is 50% of the "full scale" in terms of the inner tube diameter, the "1/4 scale" is 25% in terms of the diameter. This means that the tube cross-section and, hence, the mass flow of gas is 25% of the "full-scale" value for "1/2 scale" and 6.25% of the "full-scale" value for "1/4 scale". To treat the same amount of feed, 4 times the number of tubes will be required in the "1/2-scale" geometry and 16 times the number of tubes in the "1/4-scale" geometry. However, as the results will indicate, also the length of the reformer tubes can be reduced in a setting with reduced diameter, resulting in an overall reduced catalyst inventory and material effort.

A temperature of 900 °C was assumed for the calculation of the catalyst-bed heat-transfer properties in all investigated cases. This explains why the effective radial heat conductivity in the catalyst bed remains the same for the three different fluidized-bed temperatures investigated for 1/4 scale. The effective axial heat conductivity is considered in the model but has little effect on the results because of the significantly larger axial dimension compared to the radial dimension of the tube.

2.3. Summary of Model Equations. *2.3.1. Overall Model Structure and Boundary Conditions.* A classical pseudohomogeneous two-dimensional heat-transfer model[35] has been formulated for the cylindrical catalyst packing area in transient form and amended for reactive gas through-flow:

$$(1-\varepsilon_b)\cdot c_{p,s}\cdot\rho_p\cdot\frac{\partial T}{\partial t} = k_{r,eff}\cdot\left(\frac{\partial^2 T}{\partial r^2}+\frac{1}{r}\frac{\partial T}{\partial r}\right)+k_{a,eff}\cdot\frac{\partial^2 T}{\partial z^2}-\frac{\partial}{\partial z}\left[\sum_i (j_i\cdot H_i^*)\right] \quad (8)$$

Gas flow and composition are described in terms of species molar flux j_i and plug flow with chemical reaction is assumed for the gas phase:

$$\frac{p\cdot\varepsilon_b}{R\cdot T\cdot j_{tot}}\cdot\frac{\partial j_i}{\partial t} = -\frac{\partial j_i}{\partial z}+\frac{\rho_b}{3.6}\cdot\sum_j(\eta_j\cdot\nu_{i,j}\cdot r_j) \quad (9)$$

In eqs 8 and 9, index i stands for the gas species (CH_4, H_2O, H_2, CO, and CO_2) and index j in eq 9 stands for the three chemical reactions 1−3. The factor 3.6 converts the units used for $r_{i,j}$ in the reaction model by Xu and Froment[39] (kmol/(h·kg_{cat})) to SI units (mol/(s·kg_{cat})). In the implemented model, eq 9 is used to calculate the molar flux for CH_4 and CO_2 whereas the other three species are calculated from the elementary balance conditions for C, H, and O.

The differential equation system is numerically solved for the following boundary conditions:

$$\frac{\partial T}{\partial r}=0 \qquad \text{at } r=0 \quad (10)$$

$$k_{r,eff}\cdot\frac{\partial T}{\partial r}=h_{ov}\cdot[T_{FB}-T(r)] \qquad \text{at } r=R \quad (11)$$

$$j_i=j_{i,in} \qquad \text{at } z=0 \quad (12)$$

$$H_i^*=H_i^*(T_{g,in}) \qquad \text{at } z=0 \quad (13)$$

$$\frac{\partial T}{\partial z}=0 \qquad \text{at } z=L \quad (14)$$

Thus, the relevant model parameters to be assessed in the algebraic core of the model are the effective radial (and axial) heat conductivities in the packing ($k_{r,eff}$ and $k_{a,eff}$, respectively), the overall heat-transfer coefficient between the fluidized bed and the packing (h_{ov}) and the locally resolved effective chemical reaction rates ($\eta_j\cdot r_{i,j}$).

2.3.2. Effective Heat Conductivity in the Catalyst Packing According to Tsotsas.[38] Tube diameter to particle diameter ratio:

$$N=\frac{D}{d_p} \quad (15)$$

where d_p is the diameter of a sphere equivalent to the catalyst particles and was assumed to 6.4 mm in accordance with Wang et al.[36]

Effective porosity of the catalyst packing:[43]

$$\varepsilon_b=\varepsilon_\infty+(1-\varepsilon_\infty)\frac{0.526}{N} \quad (16)$$

Static heat conductivity of catalyst particles versus fluid heat conductivity:

$$\kappa_p=\frac{k_p}{k_f} \quad (17)$$

Effect of radiative heat transfer relative to fluid heat conductivity:[44,45]

$$\kappa_{rad}=\frac{k_{rad}}{k_f}=\frac{4\cdot\sigma\cdot d_p}{\left(\frac{2}{\varepsilon_{opt}}-1\right)}\cdot\frac{T^3}{k_f} \quad (18)$$

Heat conductivity in the packing without gas convection, simplified for a dense gas phase:[44,45]

$$\kappa_{bed}=\frac{k_{bed}}{k_f}=(1-\sqrt{1-\varepsilon_b})\cdot\varepsilon_b\cdot\left(\frac{1}{\varepsilon_b}+\kappa_{rad}\right)+\sqrt{1-\varepsilon_b}\cdot[\varphi\cdot\kappa_p+(1-\varphi)\cdot\kappa_c] \quad (19)$$

https://doi.org/10.1021/acs.energyfuels.2c01086
Energy Fuels 2022, 36, 9502−9512

$$\kappa_c = \frac{2}{n}\cdot\left[\frac{B(\kappa_p + \kappa_{rad} - 1)}{n^2\cdot\kappa_p}\cdot\ln\frac{\kappa_p + \kappa_{rad}}{B} + \frac{B+1}{2\cdot B}\cdot(\kappa_{rad} - B) - \frac{B-1}{n}\right] \quad (20)$$

$$n = 1 + \frac{\kappa_{rad} - B}{\kappa_p} \quad (21)$$

$$B = C_f\cdot\left(\frac{1-\varepsilon_b}{\varepsilon_b}\right)^{10/9} \quad (22)$$

The constant factors were chosen for ceramic spheres according to Bauer[46] as $C_f = 1.25$ and $\varphi = 0.0077$.

Effective radial heat conductivity in the catalyst packing including gas convection:[38]

$$\kappa_{r,eff} = \frac{k_{r,eff}}{k_f} = \frac{k_{bed}}{k_f} + \frac{Pe_0}{K_r} \quad (23)$$

Superficial velocity-based Peclet number:

$$Pe_0 = \frac{u_0\cdot\rho_f\cdot c_{p,f}\cdot d_p}{k_f} \quad (24)$$

The coefficient for spherical particles $K_r = 7.0$.[38]

Effective axial heat conductivity in the catalyst packing including gas convection:[38]

$$\kappa_{a,eff} = \frac{k_{a,eff}}{k_f} = \frac{k_{bed}}{k_f} + \frac{Pe_0}{2} \quad (25)$$

2.3.3. Heat Transfer from the Fluidized Bed to the Catalyst Packing. Overall heat-transfer coefficient fludized-bed−wall−catalyst packing:

$$\frac{1}{h_{ov}} = \frac{1}{h_w} + \frac{R}{k_t}\cdot\ln\frac{R+s_t}{R} + \frac{R}{R+s_t}\cdot\frac{1}{h_{FBW}} \quad (26)$$

Wall−catalyst packing heat transfer:[38]

$$Nu_w = \frac{h_w\cdot d_p}{k_f} = \left(1.3 + \frac{5}{N}\right)\cdot\frac{k_{bed}}{k_f}\cdot 0.19\cdot Re_0^{0.75}\cdot Pr^{1/3} \quad (27)$$

Heat conductivity in the reformer tube wall: $k_t = 25\ \frac{W}{mK}$.[41]

Fluidized bed to tube wall heat transfer as the sum of particle-convective, gas-convective, and radiation heat transfer:[37]

$$h_{FBW} = h_P + h_G + h_R \quad (28)$$

Particle-convective heat transfer:[37]

$$Nu_p = \frac{h_p\cdot d_p}{k_f} = (1-\varepsilon)\cdot Z\cdot[1 - e^{-(Nu_{WP,max}/C_K\cdot Z)}] \quad (29)$$

$$Z = \frac{1}{6}\cdot\frac{\rho_p\cdot c_{p,P}}{k_f}\cdot\sqrt{\frac{g\cdot d_p^3\cdot(\varepsilon - \varepsilon_{mf})}{5\cdot(1-\varepsilon_{mf})\cdot(1-\varepsilon)}} \quad (30)$$

$$Nu_{WP,max} = 4\cdot\left[\left(1 + \frac{2l}{d_p}\right)\ln\left(1 + \frac{d_p}{2l}\right) - 1\right] \quad (31)$$

$$l = 2\cdot\sqrt{\frac{2\cdot\pi\cdot R\cdot T}{M}}\cdot\frac{k_f}{p\cdot\left(2\cdot c_{p,f} - \frac{R}{M}\right)}\cdot\left(\frac{2}{\gamma} - 1\right) \quad (32)$$

$$^{10}\log\left(\frac{1}{\gamma} - 1\right) = 0.6 - \frac{\frac{1000K}{T} + 1}{C_A} \quad (33)$$

The constants C_K and C_A take the values 2.6 and 3.2, respectively.[37]

Gas-convective heat transfer:[37]

$$Nu_G = \frac{h_G\cdot d_p}{k_f} = 0.009\cdot Pr^{1/3}\cdot Ar^{1/2} \quad (34)$$

Radiation heat transfer:[37]

$$h_R = 4\cdot\varepsilon_{opt}\cdot\sigma\cdot T^3 \quad (35)$$

2.3.4. Reactions Kinetics of the SMR System According to Xu and Froment.[39] The rate equations for the three reactions 1−3 are as follows:

$$r_1 = \frac{\frac{k_1}{p_{H_2}^{2.5}}\cdot\left(p_{CH_4}\cdot p_{H_2O} - \frac{p_{H_2}^3\cdot p_{CO}}{K_{p,1}}\right)}{DEN^2} \quad (36)$$

$$r_2 = \frac{\frac{k_2}{p_{H_2}}\cdot\left(p_{CO}\cdot p_{H_2O} - \frac{p_{H_2}\cdot p_{CO_2}}{K_{p,2}}\right)}{DEN^2} \quad (37)$$

$$r_3 = \frac{\frac{k_3}{p_{H_2}^{3.5}}\cdot\left(p_{CH_4}\cdot p_{H_2O}^2 - \frac{p_{H_2}^4\cdot p_{CO_2}}{K_{p,3}}\right)}{DEN^2} \quad (38)$$

$$DEN = 1 + K_{CO}\cdot p_{CO} + K_{H_2}\cdot p_{H_2} + K_{CH_4}\cdot p_{CH_4} + \frac{K_{H_2O}\cdot p_{H_2O}}{p_{H_2}} \quad (39)$$

The partial pressure reaction equilibrium constants $K_{p,1}$, $K_{p,2}$, and $K_{p,3}$ are functions of temperature and can be calculated from ideal gas thermochemistry data[47] according to

$$\ln(K_{p,j}(T)) = -\frac{\Delta G^0_{R,j}(T)}{R\cdot T} \quad (40)$$

$$\Delta G^0_{R,j}(T) = \sum_i \nu_{i,j}\cdot H_i^*(T) - T\cdot\sum_i \nu_{i,j}\cdot S_i^0(T) \quad (41)$$

The three rate constants k_1, k_2, and k_3 are described by an Arrhenius approach:

$$k_j = k_{0,j}\cdot e^{-E_{A,j}/R\cdot T} \quad (42)$$

The Arrhenius parameters are summarized in Table 2.

Table 2. Arrhenius Parameters of Reactions 1−3[39]

reacn	reacn no.	k_0, kmol/(kgcat·h)	E_A, kJ/mol
steam reforming	(1)	4.225×10^{15}	240.1
water−gas shift	(2)	1.955×10^{6}	67.13
overall reaction	(3)	1.020×10^{15}	243.9

https://doi.org/10.1021/acs.energyfuels.2c01086
Energy Fuels 2022, 36, 9502−9512

The adsorption constants for CH_4, CO, and H_2 and the dissociative adsorption constant for H_2O for the denominator of the rate expressions are described by the van't Hoff equation:

$$K_i = K_{0,i} \cdot e^{-(\Delta H_i/R \cdot T)} \quad (43)$$

The van't Hoff parameters are summarized in Table 3.

Table 3. Van't Hoff Parameters for the Involved Gas Species[39]

species	$K_{0,i}$	ΔH_i, kJ/mol
CO	8.23×10^{-5}	−70.65
H_2	6.12×10^{-9}	−82.90
CH_4	6.65×10^{-4}	−38.28
H_2O	$1.77 \times 10^{+5}$	+88.68

The effectiveness factors η_j of the three reactions accounting for diffusional limitations within the catalyst particle were globally set to 0.02 on the basis of the findings by Xu and Froment.[40]

3. RESULTS AND DISCUSSION

3.1. Full-Scale Reformer Tube. In a first simulation, the full-scale reformer tube is simulated according to the assumptions listed in Table 1. The resulting steady state temperature distribution is shown in Figure 3.

Because of the pronounced temperature difference between tube center (tube radius = 0) and tube wall (tube radius = 0.063 m for the full-scale tube), both the chemical equilibrium gas composition of the reaction system and the reaction rates according to the Arrhenius model differ between regions in the tube center and regions close to the tube wall. This leads to the concentration deviation between center and wall shown in Figure 4. Gas conversion in the tube center is hindered by the lower local temperature in the center.

It is important to understand if the limitation for gas conversion is in the reaction rate (because of lower reaction rates at reduced temperature) or because of unfavorable equilibrium conditions at the lower temperatures. Therefore, the logarithmic deviation of the gas composition from equilibrium of reactions 1 and 2 is shown in Figure 5.

We see that chemical equilibrium of the water−gas-shift reaction 2 is reached across the whole tube cross-section after less than 33% of the total tube length (Figure 5b). For the steam reforming reaction 1, we see from Figure 5a that equilibrium is also approached toward the tube outlet about equally well across the entire tube cross-section, thus, also in the colder center region of the tube. Therefore, the conversion performance of the reformer can be considered to be limited by heat supply to a relevant degree. This is in-line with the results of the more detailed CFD model by Wang et al.,[36] where the temperature distribution and the CH_4 and H_2 distributions clearly show congruent patterns.

3.2. Effect of Reduced Tube Diameter and Increased Fluidized-Bed Temperature. The observation from section 3.1 that the heat transport toward the center of the reformer tube governs the conversion performance indicates that reformer tubes of smaller diameter reach a comparable conversion performance already after a shorter tube length. Therefore, simulation runs for tubes with 1/2 of the original inner diameter and 1/4 of the original inner diameter were carried out. The gas flow rate was reduced proportional to the tube cross-section to keep the superficial gas velocity constant (Table 1). The conversion performance and the heat flux through the tube wall are compared for the three different tube diameters over the entire original tube length of 12.5 m in Figure 6a and for the 1/4-scale geometry and the three different fluidized-bed temperatures over a length of 3.3 m in Figure 6b.

From Figure 6a it is clear that a conversion performance comparable to that of the full-scale tube is obtained at a much lower tube length for smaller tubes. This means that tubes with a smaller diameter can be built shorter, which may be key if the reformer tubes should be placed in a fluidized bed. The relevant process variables of the comparison are summarized in Table 4. The reformer tube length for conversion performance equivalent to full scale has been determined for 1/2 scale and 1/4 scale according to the graphical procedure shown in Figure 6a. If only the "equivalent" tube length is considered, less catalyst and less steel for tubes is required for the same mass flow of gas to be treated. The reduction of the tube wall thickness proportional to the tube diameter is based on the assumption of equal circumferential stress in the tube shell because of the pressure inside the tube. Additional material may be needed for fluidized-bed immersed tubes to account for abrasion losses. The density of the reformer tube alloy assumed is 8000 kg/m^3.[41] A further reduction of the conversion-equivalent tube length can be obtained if the fluidized-bed temperature is increased (Figure 6b).

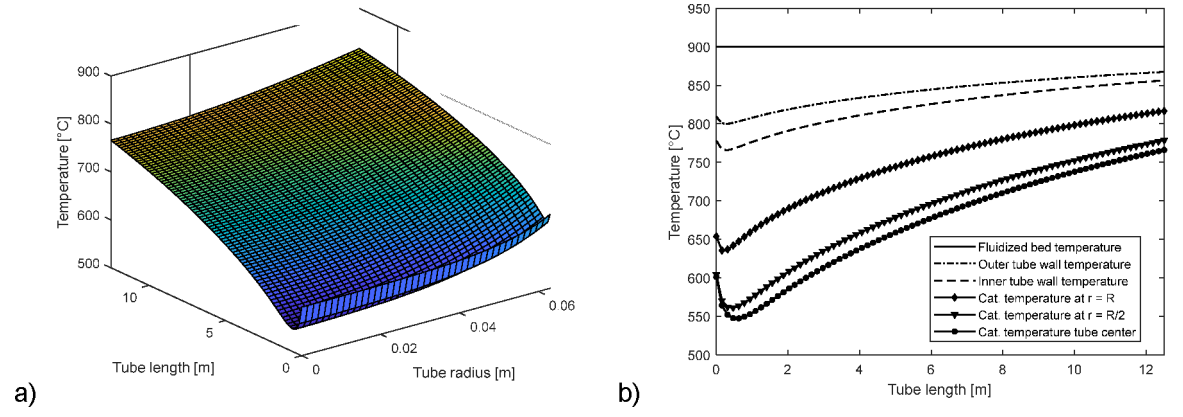

Figure 3. Steady state temperature distribution inside the catalyst packing (a) and including the surrounding fluidized bed and tube shell (b) for the full-scale reformer tube.

https://doi.org/10.1021/acs.energyfuels.2c01086
Energy Fuels 2022, 36, 9502−9512

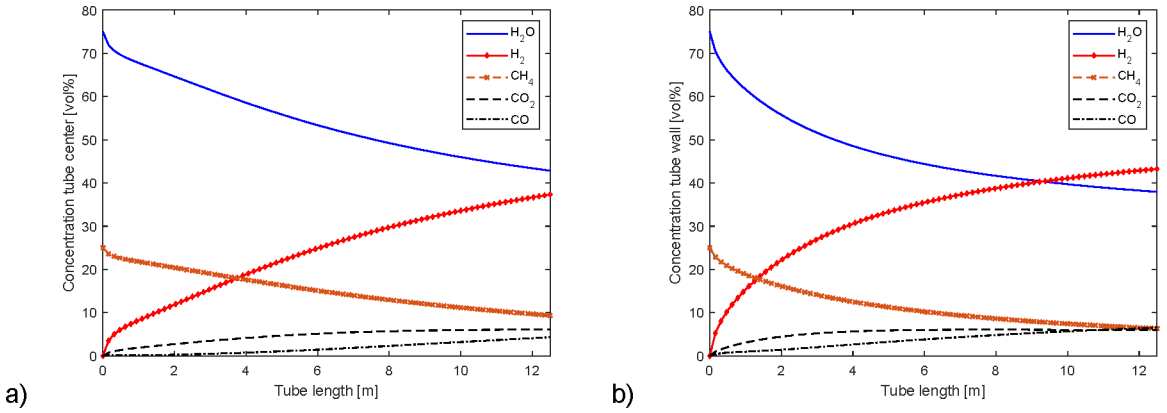

Figure 4. Steady state gas composition distribution along the tube length in the tube center (a) and at the tube wall (b) for the full-scale reformer tube.

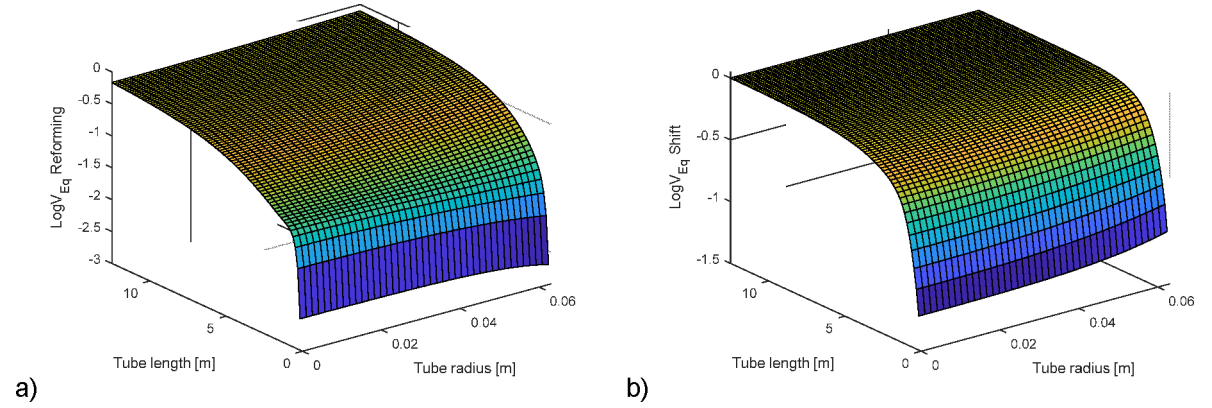

Figure 5. Logarithm of the local deviation from equilibrium of the reforming reaction (a) and of the water−gas-shift reaction (b). A value of zero means equilibrium is reached, and values <0 mean the local gas composition is on the reactants' side of the reaction equilibrium.

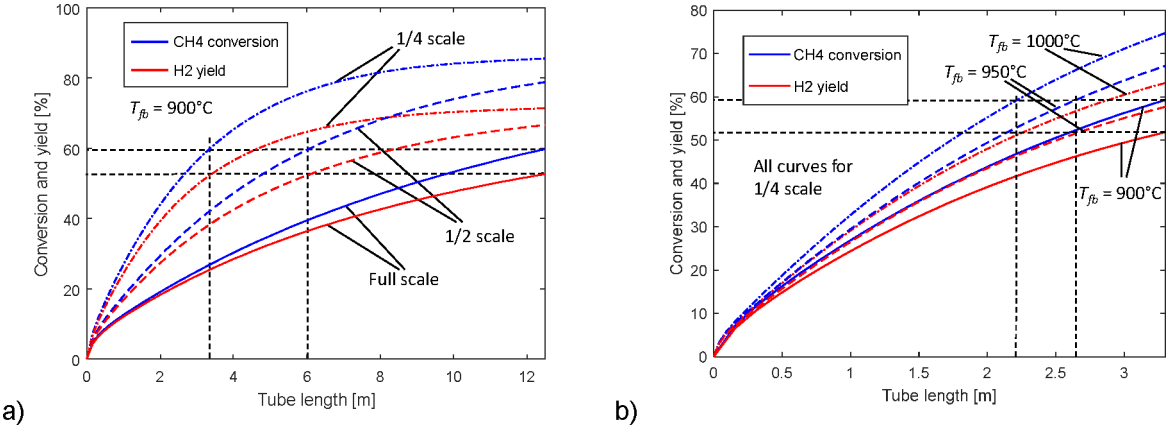

Figure 6. Conversion performance in terms of the CH_4 conversion (blue lines) and the H_2 yield (red lines) for three different tube diameters ("full scale", 126 mm; 1/2 scale, 63 mm; 1/4 scale, 31.5 mm) (a) and for 1/4 scale and three different fluidized-bed temperatures (b).

3.3. Discussion. The model results, obtained with all the simplifications and taken assumptions indicate that reformer tubes of smaller diameter could be short enough to allow for insertion in fluidized beds. This is seen as the main message from the present contribution. There are several limitations to the outcome of this work that could be addressed by further research:

- What is the real effective heat transfer between the fluidized bed and tube wall and to and within the catalyst bed?

For the results shown above, models suggested in the state-of-the-art literature were used to predict the heat transfer using a globally applied h_w model[35,38] for the heat transfer within the fixed bed of the catalyst. A relevant contribution comes from radiation heat transfer at the operating temperature of the reformer, which indicates that the effective heat conductivity is dependent on the local temperature.

- What are the real mass-transfer-limited reaction rates of the governing reactions?

https://doi.org/10.1021/acs.energyfuels.2c01086
Energy Fuels 2022, 36, 9502−9512

Table 4. Comparison of the Three Investigated Tube Diameters

parameter	unit	full scale	1/2 scale	1/4 scale		
reformer tube inner diameter	mm	126	63	31.5		
reformer tube length simulated	m	12.5	12.5	12.5		
fluidized-bed temperature	°C	900	900	900	950	1000
CH_4 conversion after 12.5 m	%	59.7	78.7	85.4	n.a.	n.a.
H_2 yield after 12.5 m	%	52.6	66.6	71.3	n.a.	n.a.
reformer tube length for conversion performance equivalent to full scale	m	12.5	6.0	3.3	2.6	2.2
equivalent number of tubes		1	4	16	16	16
equivalent catalyst-bed volume	m^3	0.156	0.075	0.041	0.032	0.027
tube shell thickness	mm	10	5	2.5	2.5	2.5
tube shell material mass		396	190	105	82	70

The length reduction effect will be reduced if the reactions are slower making a sufficient gas-catalyst contact time more relevant. In the present work, global effectiveness factors of 0.02 were applied to the three intrinsic governing reactions according to Xu and Foment.[39,40] A more detailed reactor model predicting local effectiveness factors could improve the prediction quality.

4. CONCLUSION

Though the industrially established reformer tube design with 12.5 m long and 12.6 cm inner diameter tubes may be an economic optimum for flame-heated reactive furnaces, the choice of tube diameter could be different for reformer tubes heated by fluidized-bed reactors. The outcome of the present plausibility investigation shows that, because heat transfer is a relevant limitation to the process, smaller tube diameters will lead to significantly shorter tubes. This may be essential for placing the tubes inside a fluidized bed.

Further reactor design studies will be necessary with more precise description of the governing phenomena, also on the side of the CLC process to come to final conclusions with respect to the practical feasibility of the, in terms of process design highly promising, marriage between CLC and SMR.

AUTHOR INFORMATION

Corresponding Author

Tobias Pröll − *University of Natural Resources and Life Sciences, Vienna, 1190 Vienna, Austria;* orcid.org/0000-0001-6240-1916; Email: tobias.proell@boku.ac.at

Author

Anders Lyngfelt − *Chalmers University of Technology, 412 96 Göteborg, Sweden;* orcid.org/0000-0002-9561-6574

Complete contact information is available at: https://pubs.acs.org/10.1021/acs.energyfuels.2c01086

Notes

The authors declare no competing financial interest.

NOMENCLATURE

Ar	Archimedes number $Ar = \frac{\rho_f \cdot (\rho_p - \rho_f) \cdot g \cdot d_p^3}{\mu_f^2}$
B	intermediate expression in eqs 20 and 21
C_A	constant in eq 33
C_f	shape factor in eq 19
C_K	constant in eq 29
c_p	specific heat capacity. J/(kg·K)
D	inner diameter of reformer tube: $D = 2 \cdot R$, m
DEN	denominator term in reaction rate expression
d_p	hydrodynamically relevant particle diameter, m
$E_{A,j}$	activation energy in Arrhenius equation of reaction j, J/mol
ΔG_R^0	standard pressure Gibbs free enthalpy of reaction, J/mol
h	heat-transfer coefficient, W/(m^2·K)
H_i^*	conventional molar enthalpy of species i, J/mol
ΔH_i	adsorption enthalpy in van't Hoff equation for species i, J/mol
j_i	molar flux of species i in axial direction, mol/(m^2·s)
j_{H_2}	molar flux of hydrogen in axial direction, mol/(m^2·s)
k	heat conductivity, W/(m·K)
k_j	reaction rate coefficient of reaction j, kmol/(kg_{cat}·h)
$k_{0,j}$	pre-exponential factor in Arrhenius equation of reaction j, kmol/(kg_{cat}·h)
K_i	adsorption equilibrium constant for species i
$K_{0,i}$	pre-exponential factor in van't Hoff equation for species i
K_p	partial pressure equilibrium constant, a function of temperature
K_r	fluid mixing coefficient in eq 23: $K_r = 7$ for spheres
L	reformer tube length, m
n	intermediate expression in eqs 20 and 21
$\dot{n}_i$	molar flow of species i, mol/s
N	tube to particle diameter ratio
Nu	Nusselt number $Nu = \frac{h \cdot d_p}{k_f}$
$Nu_{WP,max}$	maximum wall−particle heat-transfer Nusselt number
p	overall pressure, Pa
p_i	dimensionless partial pressure of species i relative to p_0
p_0	standard pressure p_0 = 1 bar = 10^5 Pa, Pa
Pe_0	superficial velocity Peclet number (eq 24)
Pr	Prandtl number $Pr = \frac{\mu_f \cdot c_{p,f}}{k_f}$
r	radial coordinate, m
r_j	reaction rate of reaction j according to Xu and Froment,[39] kmol/(kg_{cat}·h)
R	inner tube radius, m
Re_0	superficial velocity particle Reynolds number $Re_0 = \frac{u_0 \cdot d_p \cdot \rho_f}{\mu_f}$
s_t	thickness of reformer tube wall, m
S_i^0	standard pressure entropy of species i, J/(mol·K)
t	time, s
T	temperature, K
u_0	superficial gas velocity, m/s
V_{eq}	deviation from chemical equilibrium according to eqs 6 and 7
X_{CH_4}	methane conversion
Y_{H_2}	hydrogen yield
z	length coordinate, m
Z	intermediate expression in eqs 29 and 30

https://doi.org/10.1021/acs.energyfuels.2c01086
Energy Fuels 2022, 36, 9502−9512

GREEK SYMBOLS

γ intermediate expression in eqs 32 and 33
ε voidage in fluidized bed
ε_b mean voidage in catalyst packing
ε_∞ voidage in catalyst packing far from the tube wall
ε_{opt} emissivity coefficient of heat radiation
η_j effectiveness factor of reaction j
κ heat conductivity relative to fluid heat conductivity
κ_c intermediate expression in eqs 19 and 20
μ_f dynamic viscosity of the fluid, Pa·s
$\nu_{i,j}$ stoichiometric coefficient of species i in reaction j
ρ density, kg/m^3
σ Stefan−Boltzmann constant: $\sigma = 5.67 \times 10^{-8}$ W/(m^2·K^4)
φ shape factor in eq 19

INDICES

a referring to axial properties within catalyst bed
b referring to bulk volume of catalyst bed
bed referring to catalyst bed without gas convection effects
eff effective overall heat transport within the catalyst packing
f referring to fluid
FB referring to fluidized bed
FBW fluidized-bed−wall interface
g referring to gas stream
G indicating gas-convective heat transfer
i referring to gas species
in referring to gas stream at the tube inlet
j referring to reactions
mf referring to minimum fluidization conditions
ov overall heat-transfer fluidized-bed−tube-wall−catalyst packing
p referring to particles (catalyst or bed material)
P indicating particle-convective heat transfer
r referring to radial properties within catalyst bed
R indicating radiation heat transfer (fluidized bed)
rad indicating radiation heat transfer (catalyst packing)
s referring to solids (catalyst particles)
t referring to reformer tube
tot referring to total gas flow (all species)
w tube-wall−catalyst-bed interface

REFERENCES

(1) Dybkjaer, I. Tubular reforming and autothermal reforming of natural gas − an overview of available processes. *Fuel Proc. Technol.* **1995**, *42*, 85−107.
(2) Quang, D. V.; Rabindran, A. V.; Hadri, N. E.; Abu-Zahra, M. R. M. Reduction in the Regeneration Energy of CO2 Capture Process by Impregnating Amine Solvent onto Precipitated Silica. *Eur. Sci. J.* **2013**, *9* (30), 82−102.
(3) Rydén, M.; Lyngfelt, A. Using steam reforming to produce hydrogen with carbon dioxide capture by chemical-looping combustion. *Int. J. Hydrogen Energy* **2006**, *31*, 1271−1283.
(4) Kaiser, S. (Director Technology Andritz AG Power Boilers), personal communication, October 21, 2021.
(5) Lyngfelt, A.; Pallarès, D.; Linderholm, C.; Lind, F.; Thunman, H.; Leckner, B. Achieving Adequate Circulation in Chemical-Looping Combustion − Design proposal for 200 MWth Chemical Looping Combustion Circulating Fluidized Bed Boiler, accepted for publication in. *Energy Fuels* **2022**, DOI: 10.1021/acs.energyfuels.1c03615.
(6) Stenberg, V.; Spallina, V.; Mattisson, T.; Rydén, M. Techno-economic analysis of H2 production processes using fluidized bed heat exchangers with steam reforming − Part 2: Chemical-looping combustion. *Int. J. Hydrogen Energy* **2021**, *46*, 25355−25375.
(7) Lyngfelt, A. Chemical Looping Combustion: Status and Development Challenges. *Energy Fuels* **2020**, *34*, 9077−9093.
(8) Lyngfelt, A.; Brink, A.; Langørgen, Ø.; Mattisson, T.; Rydén, M.; Linderholm, C. 11,000 h of Chemical-Looping Combustion Operation − Where Are We and Where Do We Want to Go? *International Journal of Greenhouse Gas Control* **2019**, *88*, 38−56.
(9) Lyngfelt, A.; Leckner, B. A 1000 MWth Boiler for Chemical-Looping Combustion of Solid Fuels − Discussion of Design and Costs. *Applied Energy* **2015**, *157*, 475−487.
(10) Mattisson, T.; Lyngfelt, A.; Leion, H. Chemical-looping with oxygen uncoupling for combustion of solid fuels. *International Journal of Greenhouse Gas Control* **2009**, *3*, 11−19.
(11) Adanez, J.; Abad, A.; Garcia-Labiano, F.; Gayan, P.; de Diego, L. Progress in chemical-looping combustion and reforming technologies. *Progress in energy and combustion science* **2012**, *38*, 215−282.
(12) Källén, M.; Rydén, M.; Dueso, C.; Mattisson, T.; Lyngfelt, A. CaMn0.9Mg0.1O3-δ as Oxygen Carrier in a Gas-Fired 10 kWth Chemical-Looping Combustion Unit. *Ind. Eng. Chem. Res.* **2013**, *52*, 6923−6932.
(13) Hallberg, P.; Hanning, M.; Rydén, M.; Mattisson, T.; Lyngfelt, A. Investigation of a calcium Manganite as oxygen carrier during 99 h of operation of Chemical-Looping Combustion in a 10 kW unit. *International Journal of Greenhouse Gas Control* **2016**, *53*, 222−229.
(14) Rydén, M.; Lyngfelt, A.; Mattisson, T. CaMn0.875Ti0.125O3 as oxygen carrier for chemical-looping combustion with oxygen uncoupling (CLOU) − experiments in continuously operating fluidized bed reactor system. *Int. J. Greenhouse Gas Control* **2011**, *5* (2), 356−366.
(15) Hallberg, P.; Källén, M.; Jing, D.; Snikjers, F.; van Noyen, J.; Rydén, M.; Lyngfelt, A. Experimental investigation of CaMnO3-δ based oxygen carriers used in continuous Chemical-Looping Combustion. *Int. J. Chem. Eng.* **2014**, No. 412517.
(16) Hallberg, P.; Rydén, M.; Mattisson, T.; Lyngfelt, A. CaMnO3-δ made from low cost material examined as oxygen carrier in Chemical-Looping Combustion. *Energy Procedia* **2014**, *63*, 80−86.
(17) Schmitz, M.; Linderholm, C.; Lyngfelt, A. Chemical Looping Combustion of Sulfurous Solid Fuels using Calcium Manganite as Oxygen Carrier. *Energy Procedia* **2014**, *63*, 140−152.
(18) Schmitz, M.; Linderholm, C. Performance of calcium Manganite as oxygen carrier in chemical looping combustion of biomass in a 10 kW pilot. *Applied Energy* **2016**, *169*, 729−737.
(19) Cabello, A.; Abad, A.; Gayán, P.; de Diego, L. F.; García-Labiano, F.; Adánez, J. Effect of operating conditions and H2S presence on the performance of CaMg0.1Mn0.9O3-δ perovskite material in chemical looping combustion (CLC). *Energy Fuels* **2014**, *28*, 1262−1274.
(20) Mattisson, T.; Adánez, J.; Mayer, K.; Snijkers, F.; Williams, G.; Wesker, E.; Bertsch, O.; Lyngfelt, A. Innovative Oxygen Carriers Uplifting Chemical-looping Combustion. *Energy Procedia* **2014**, *63*, 113−130.
(21) Mayer, K.; Penthor, S.; Pröll, T.; Hofbauer, H. The different demands of oxygen carriers on the reactor system of a CLC plant − Results of oxygen carrier testing in a 120 kWth pilot plant. *Applied Energy* **2015**, *157*, 323−329.
(22) Ohlemüller, P.; Reitz, M.; Ströhle, J.; Epple, B. Operation of a 1 MWth chemical looping pilot plant with natural gas. Presented at High Temperature Solid Looping Cycles Network, Luleå, Sweden, 2017.
(23) Ohlemüller, P.; Reitz, M.; Ströhle, J.; Epple, B. Operation of a 1 MWth chemical looping pilot plant with natural gas. Presented at 9th Trondheim Conference on CO2 Capture, Transport and Storage, Trondheim, Norway, 2017.
(24) Tilland, A.; Lambert, A.; Pelletant, W.; Chiche, D.; Bounie, C.; Bertholin, S. Comparison of two oxygen carriers performances for Chemical Looping Combustion application. Presented at 9th Trondheim Conference on CO2 Capture, Transport and Storage, Trondheim, Norway, 2017.
(25) Moldenhauer, P.; Rydén, M.; Mattisson, T.; Jamal, A.; Lyngfelt, A. Chemical-Looping Combustion with Heavy Liquid Fuels in a 10 kW Pilot Plant. *Fuel Process. Technol.* **2017**, *156*, 124−137.

https://doi.org/10.1021/acs.energyfuels.2c01086
Energy Fuels 2022, 36, 9502−9512

(26) Penthor, S.; Mattisson, T.; Adánez, J.; Bertolin, S.; Masi, E.; Larring, Y.; Langørgen, Ø.; Ströhle, J.; Snijkers, F.; Geerts, L.; Albertsen, K.; Williams, G.; Bertsch, O.; Authier, O.; Dávila, Y.; Yazdanpanah, M.; Pröll, T.; Lyngfelt, A.; Hofbauer, H. The EU-FP7 project SUCCESS − Scale-up of oxygen carrier for chemical looping combustion using environmentally sustainable materials. *Energy Procedia* **2017**, *114*, 395−406.
(27) Sundqvist, S. Manganese ores as oxygen carriers for chemical-looping combustion, *Ph.D. Thesis*. Dept. of Chemical and Biological Engineering, Chalmers University of Technology, Göteborg, Sweden, 2017.
(28) Dickmeis, J.; Kather, A. Offgas Treatment downstream the Gas Processing Unit of a Pulverised Coal-Fired Oxyfuel Power Plant with Polymeric Membranes and Pressure Swing Adsorption. *Energy Procedia* **2013**, *37*, 1301−1311.
(29) Gogolev, I.; Linderholm, C.; Gall, D.; Schmitz, M.; Mattisson, T.; Pettersson, J. B. C.; Lyngfelt, A. Chemical-Looping Combustion in a 100 kW Unit Using a Mixture of Synthetic and Natural Oxygen Carriers − Operational Results and Fate of Biomass Fuel Alkali. *International Journal of Greenhouse Gas Control* **2019**, *88*, 371−382.
(30) Linderholm, C.; Schmitz, M. Chemical-Looping Combustion of Solid Fuels in a 100 kW Dual Circulating Fluidized Bed System using Iron Ore as Oxygen Carrier. *Journal of Environmental Chemical Engineering* **2016**, *4*, 1029−1039.
(31) Linderholm, C.; Schmitz, M.; Biermann, M.; Hanning, M.; Lyngfelt, A. Chemical-looping combustion of solid fuel in a 100 kW unit using sintered manganese ore as oxygen carrier. *International Journal of Greenhouse Gas Control* **2017**, *65*, 170−181.
(32) Linderholm, C.; Schmitz, M.; Knutsson, P.; Källén, M.; Lyngfelt, A. Use of low-volatile fuels in a 100 kW chemical-looping combustor. *Energy Fuels* **2014**, *28*, 5942−5952.
(33) Markström, P.; Linderholm, C.; Lyngfelt, A. Chemical-looping combustion of solid fuels - Design and operation of a 100 kW unit with bituminous coal. *International Journal of Greenhouse Gas Control* **2013**, *15*, 150−162.
(34) Schmitz, M.; Linderholm, C. Chemical looping combustion of biomass in 10 and 100 kW pilots - Analysis of conversion and lifetime using a sintered manganese ore. *Fuel* **2018**, *231*, 73−84.
(35) Dixon, A. G. Fixed bed catalytic reactor modelling − The radial heat transfer problem. *Can. J. Chem. Eng.* **2012**, *90*, 507−527.
(36) Wang, J.; Wei, S.; Wang, Q.; Sundén, B. Transient numerical modelling and model predictive control of an industrial-scale steam methane reforming reactor. *Int. J. Hydrogen Energy* **2021**, *46*, 15241−15256.
(37) Martin, H. *Heat transfer in fluidized beds, Section M5 in VDI Heat Atlas*; Springer: Berlin, 2011 (in German); DOI DOI: 10.1007/978-3-642-19981-3.
(38) Tsotsas, E. *Wärmeleitung und Dispersion in durchströmten Schüttungen, Section M7 in VDI Heat Atlas*; Springer: Berlin, 2011 (in German); DOI DOI: 10.1007/978-3-642-19981-3.
(39) Xu, J.; Froment, G. F. Methane Steam Reforming, Methanation and Water-Gas Shift: I. Intrinsic Kinetics. *AIChE J.* **1989**, *35*, 88−96.
(40) Xu, J.; Froment, G. F. Methane Steam Reforming: II. Diffusional limitations and reactor simulation. *AIChE J.* **1989**, *35*, 97−103.
(41) Dixon, A. G. Local transport and reaction rates in a fixed bed reactor tube: Endothermic steam methane reforming. *Chem. Eng. Sci.* **2017**, *168*, 156−177.
(42) Pedernera, M. N.; Pina, J.; Borio, D. O.; Bucalá, V. Use of a heterogeneous two-dimensional model to improve the primary steam reformer performance. *Chem. Eng. J.* **2003**, *94*, 29−40.
(43) Sonntag, G. Einfluss des Lückenvolumens auf den Druckverlust in gasdurchströmten Füllkörpersäulen. *Chem.-Ing.-Technol.* **1960**, *32*, 317−329. (in German).
(44) Zehner, P.; Schlünder, E. U. Einfluss der Wärmestrahlung und des Druckes auf den Wärmetransport in nicht durchströmten Schüttungen. *Chem.-Ing.-Technol.* **1972**, *44*, 1303−1308. (in German).
(45) Bauer, R.; Schlünder, E. U. Effective radial thermal conductivity of packings in gas flow. *Int. Chem. Eng.* **1978**, *18*, 189−204.
(46) Bauer, R. *Effektive radiale Wärmeleitfähigkeit gasdurchströmter Schüttungen mit Partikeln uinterschiedlicher Form und Größenverteilung*; VDI-Forschungsheft 582; VDI Verlag: Düsseldorf, 1977 (in German).
(47) Burcat, A.; Ruscic, B. *Third Millennium Ideal Gas and Condensed Phase Thermochemical Database for Combustion with Updates from Active Thermochemical Tables*; Argonne National Laboratory Report no. ANL-05/20; ANL, 2005.

https://doi.org/10.1021/acs.energyfuels.2c01086
Energy Fuels 2022, 36, 9502−9512